ORIGINAL PAPER

Adsorption properties and inhibition of mild steel corrosion in hydrochloric acid solution by ceftobiprole

Ashish Kumar Singh · M. A. Quraishi

Abstract The inhibition effect of ceftobiprole against the corrosion of mild steel in 1 M HCl solution was studied by weight loss, electrochemical impedance spectroscopy (EIS), potentiodynamic polarization and atomic force microscopy techniques. Inhibition efficiency increased with inhibitor concentration where as decreased with acid concentration. Data obtained from EIS studies were analyzed to model the corrosion inhibition process through appropriate equivalent circuit models. The adsorption of ceftobiprole obeyed Langmuir adsorption isotherm. Both thermodynamic and activation parameters were calculated and discussed. Polarization curves indicated that they are mixed type of inhibitors. Polarization curves showed that ceftobiprole act as mixed-type inhibitor. The results obtained from weight loss, EIS and Potentiodynamic polarization are in good agreement.

Keywords Corrosion inhibition · AFM · Thermodynamic parameters · EIS

1 Introduction

Organic inhibitors were applied extensively to protect metals from corrosion in many aggressive acidic media (e.g., in the acid pickling and cleaning processes of metals) [1–4]. Organic compounds containing N, S and O atoms [5–14] were found to be good corrosion inhibitors of metals particularly for active metals like Fe, Zn, and Mg

etc. The effectiveness of theses compounds as corrosion inhibitors has been interpreted in terms of their molecular structure, molecular size, and molecular mass, hetero-atoms present and adsorptive tendencies [15]. Under certain conditions, the electronic structure of the organic inhibitors has a key influence on the corrosion inhibition efficiency to the metal. The inhibitors influence the kinetics of the electrochemical reactions which constitute the corrosion process and thereby modify the metal dissolution in acids. The existing data show that most organic inhibitors act by adsorption on the metal surface. They change the structure of the electrical double layer by adsorption on the metal surface. Quite a number of studies have been carried out in determination of adsorptivity of various compounds at the electrode/solution interface [16–18].

A large number of organic compounds were studied as corrosion inhibitor, uunfortunately most of the organic inhibitors used are very expensive and health hazards. Their toxic properties limit their field of application. Thus, it remains an important object to find cost-effective and non-hazardous inhibitors for the protection of metals against corrosion. In this connection, the influences of non-toxic organic compounds and drugs on the corrosion of metals in acid media were investigated by several authors [19–27].

2 Experimental

2.1 Materials

Mild steel strips composed of (wt%) C = 0.17, Mn = 0.46, Si = 0.26, S = 0.017, P = 0.019 and balance Fe were used for weight loss as well as electrochemical measurements. The rectangular specimens with dimension

A. K. Singh · M. A. Quraishi (✉)
Department of Applied Chemistry, Institute of Technology,
Banaras Hindu University, Varanasi 221 005, India
e-mail: maquraishi@rediffmail.com;
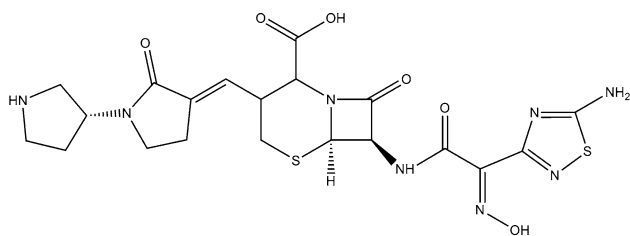maquraishi.apc@itbhu.ac.in

Fig. 1 Molecular structure of ceftobiprole

$2.5 \times 2.0 \times 0.025$ cm were used in weight loss experiments and of size 1.0 cm $\times$ 1.0 cm (exposed) with a 7.5 cm long stem (isolated with commercially available lacquer) were used for electrochemical measurements. The solutions (1 M HCl) were prepared by dilution of an analytical grade HCl with double distilled water. The molecular structure of ceftobiprole is shown in Fig. 1. The inhibitor concentration in the weight loss and electrochemical study was in the range of 0.93×10^{-4}–9.31×10^{-4} M.

2.2 Weight loss studies

Weight loss experiments were done according to the method described previously [28]. Weight loss measurements were performed at 308 K (except for temperature effect) for 3 h (except for immersion time effect) by immersing the mild steel coupons into acid solution (100 mL) without and with various amounts of inhibitors.

The inhibition efficiency (μ_{WL} %) and surface coverage (θ) was determined by using following equation:

$$\theta = \frac{w_o - w_i}{w_o} \tag{1}$$

$$\mu_{WL}\% = \frac{w_0 - w_i}{w_0} \times 100 \tag{2}$$

where, w_i and w_0 are the weight loss value in presence and absence of inhibitors, respectively.

2.3 Electrochemical measurements

The electrochemical studies were performed using a three electrode cell assembly at room temperature [29, 30]. The mild steel of 1 cm^2 was the working electrode, platinum electrode was used as an auxiliary electrode, and standard calomel electrode (SCE) was used as reference electrode. All potentials were measured versus SCE. The polarization and impedance studies were carried out using Gamry Potentiostat/Galvanostat (model 300) with EIS software, Gamry-Instruments Inc., USA.

Tafel curves were obtained by changing the electrode potential automatically from -250 to $+250$ mV versus corrosion potential (E_{corr}) at a scan rate of 1 mV s^{-1}. EIS measurements were carried out in a frequency range from 100,000 Hz to 0.01 Hz under potentiodynamic conditions, with amplitude of 10 mV peak-to-peak, using AC signal at E_{corr}. All experiments were measured after immersion for 30 min in 1 M HCl with and without addition of inhibitor.

The linear polarization study was carried out from cathodic potential of -20 mV versus OCP to an anodic potential of $+20$ mV versus OCP with a scan rate 0.125 mV s^{-1} to study the polarization resistance (R_p).

2.4 Atomic force microscopy

The surface morphology of mild steel specimen was investigated by using atomic force microscope (AFM). Atomic force microscopy was performed using a NT-MDT multimode AFM, Russia, controlled by Solver scanning probe microscope controller. Semi-contact mode was used with the tip mounted on 100 μm long, single beam cantilever with resonant frequency in the range of 240,000–255,000 Hz, and the corresponding spring constant of 11.5 N m^{-1} with NOVA programme used for image rendering. The mild steel strips of $1.0 \times 1.0 \times 0.025$ cm sizes were prepared as described in Sect. 2.2. After immersion in 1 M HCl with and without addition of 7.45×10^{-4} M ceftobiprole at 308 K for 3 h, the specimen were cleaned with distilled water, dried and then used for AFM.

3 Result and discussion

3.1 Weight loss studies

3.1.1 Effect of inhibitor concentration

The value of inhibition efficiency (μ_{WL} %) and corrosion rate (C_R) obtained from weight loss method at different concentrations in 1 M HCl at different temperatures are presented in Table 1. The optimum concentration of inhibitor was evaluated based on their inhibition efficiency. The inhibition behaviour of ceftobiprole against concentration is given in Fig. 2a.

3.1.2 Effect of immersion time

The variation of inhibition efficiency of ceftobiprole with immersion time is shown in Fig. 2b. The inhibition efficiency of the inhibitor was found to decrease with time, suggesting that the inhibitor start to desorb with increasing time.

3.1.3 Effect of temperature

In order to study the effect of temperature on the inhibition characteristic of ceftobiprole, weight loss measurements

were performed at different temperatures from 308 to 338 K in absence and presence of different concentrations of ceftobiprole for 3 h immersion time and the effect of

Table 1 Corrosion rate and Inhibition efficiency values for the corrosion of mild steel in aqueous solution of 1 M HCl in absence and presence of different concentrations of ceftobiprole from weight loss measurements at different temperatures

Concentration of inhibitor ($M \times 10^{-4}$)	Temperature (K)	Corrosion rate (mm y^{-1})	$\mu_{WL}\%$
1 M HCl	308	40.4	–
	318	58.2	–
	328	100.9	–
	338	174.5	–
0.93	308	12.5	69.0
	318	22.1	61.9
	328	47.4	52.9
	338	101.4	41.9
1.86	308	7.8	80.6
	318	15.1	73.9
	328	36.3	63.9
	338	85.5	50.9
3.72	308	6.0	84.9
	318	13.4	77.0
	328	32.3	67.9
	338	80.3	53.9
5.59	308	4.6	88.5
	318	9.9	83.0
	328	25.9	74.2
	338	61.4	64.8
7.45	308	3.3	91.6
	318	7.9	86.4
	328	21.3	78.9
	338	52.9	69.7
9.31	308	3.2	92.2
	318	7.9	86.4
	328	21.0	79.2
	338	51.7	70.4

temperature on inhibition efficiency at different inhibitor concentration is shown in Fig. 2a.

As detected from Fig. 2a, inhibition efficiency decreased in the presence of optimum concentration of ceftobiprole in studied temperature range which indicated desorption of inhibitor molecule with increasing temperature. However, this decrease in inhibition efficiency is small at higher inhibitor concentration.

The dependence of corrosion rate at temperature can be expressed by Arrhenius equation and transition state equation [31, 32]:

$$\log(C_R) = \frac{-E_a}{2.303RT} + \log \lambda \qquad (3)$$

$$C_R = \frac{RT}{Nh} \exp\left(\frac{\Delta S^*}{R}\right) \exp\left(-\frac{\Delta H^*}{RT}\right) \qquad (4)$$

where E_a apparent activation energy, λ the pre-exponential factor, ΔH^* the apparent enthalpy of activation, ΔS^* the apparent entropy of activation, h Planck's constant and N the Avogadro number, respectively.

The apparent activation energy and pre-exponential factors for a wide range of concentration of ceftobiprole can be calculated by linear regression between $\log C_R$ and $1/T$, the results were shown in Table 2. All the linear regression coefficients are close to 1, indicating that corrosion of mild steel in hydrochloric acid can be explained using the kinetic model. Figure 3a depicted an Arrhenius plots for mild steel immersed in 1 M HCl in presence of different concentration of ceftobiprole. The plots obtained are straight lines and the slope of each straight line gives its apparent activation energy. Table 2 summarized E_a values for a wide range of concentration of ceftobiprole. Inspection of Table 2 showed that apparent activation energy increased with increasing concentration of ceftobiprole. The increase in E_a could be interpreted as the physical adsorption. Szauer and Brand [33] explained that the increase in activation energy can be attributed to an appreciable decrease in the adsorption of the inhibitor on the mild steel surface with increase in temperature and a corresponding increase in corrosion rates occurs due to the

Fig. 2 Variation of inhibition efficiency in 1 M HCl on mild steel of surface area 10 cm² with **a** different conc. of ceftobiprole inhibitor at different temperatures and **b** immersion time at 7.45×10^{-4} M conc.
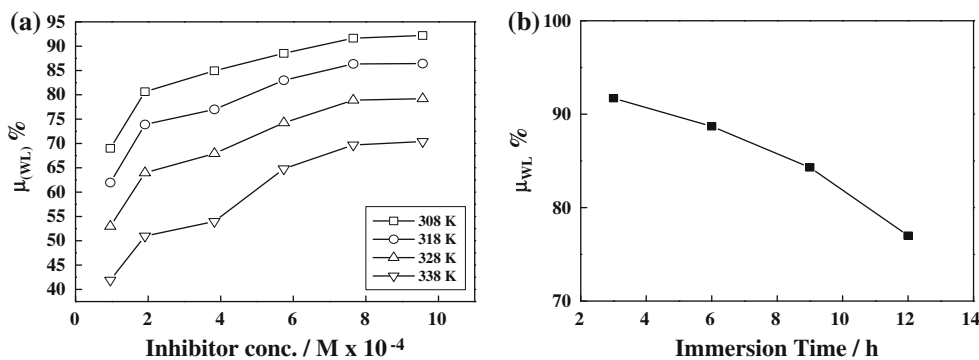
Table 2 Thermodynamic activation parameters for mild steel in 1 M HCl in absence and presence of different concentrations of ceftobiprole

Name of inhibitor	Conc. of inhibitor ($M \times 10^{-4}$)	E_a (kJ mol^{-1})	λ (mg cm^{-2})	ΔH^* (kJ mol^{-1})	ΔS^* (J mol^{-1} K^{-1})
1 M HCl	–	42.21	5.31×10^{8}	39.57	−86.75
Ceftobiprole	0.93	60.16	1.79×10^{11}	57.50	−38.38
	1.86	68.85	3.30×10^{12}	66.19	−14.17
	3.72	74.65	1.80×10^{13}	71.13	−0.04
	5.59	74.61	1.87×10^{13}	71.95	0.27
	7.45	79.13	8.07×10^{13}	76.48	12.43
	9.31	78.74	6.89×10^{13}	76.08	11.09

fact that greater area of metal is exposed to the acid environment.

According to Eq. 3, corrosion rate (C_R) is being effected by both E_a and λ. In general, the influence of E_a on the mild steel corrosion was higher than that of λ on the mild steel corrosion. However, if the variation in λ was drastically higher than that of E_a, the value of λ might be the dominant factor to determine the mild steel corrosion. In the present case, E_a and λ increased with concentration (the higher E_a and lower λ led to lower corrosion rate). As it can be seen from Table 1, the corrosion rate of steel decreased with increasing concentration; hence, it is clear that increment of E_a is the decisive factor affecting the corrosion rate of mild steel in 1 M HCl.

The results obtained in the study could be explained by the mechanism proposed by Riggs and Hurd [34]. The authors proposed a mechanism which can be applied to explain the result of present study. The authors suggested that the corrosion rate, $-d(Fe)/dt$, can be expressed by sum of two rates: $-d(Fe)/dt = k_1(1 - \theta) + k_2\theta$, where k_1 and k_2 are the rate constants for the uninhibited reaction and completely covered surface, respectively, and θ is the fraction of surface covered by adsorbed inhibitor.

To confirm this proposal, the C_R/θ was plotted against the $1 - \theta/\theta$ for each temperature tested. The values of k_1 and k_2 can be calculated from slopes and intercept of straight lines, respectively. The values of k_1 and k_2

calculated at different temperature are presented in Table 3. The corrosion rate of uninhibited mild steel, 40.4–174.5 mm y^{-1} determined using weight loss method shows good agreement with the results obtained from k_1 and the hypothesis is justified.

The Fe (Inh)$_{ads}$, reaction intermediates [35]: Fe + Inh ↔ Fe-(Inh)$_{ads}$ + Fe^{n+} + ne$^-$ + Inh can explain the inhibition mechanism. At first, when there is not enough Fe (Inh)$_{ads}$ to cover the metal surface, because the inhibitor concentration is low or because the adsorption rate is slow, metal dissolution takes place on the mild steel surface free of Fe (Inh)$_{ads}$. With high inhibitor concentration a compact and coherent inhibitor film is formed on the mild steel which reduces chemical attacks on the metal.

In many systems k_2 may be so small that $k_2\theta$ may be negligible. When θ becomes quite large (>0.9), very small increase in k_2 causes the term $k_1 (1 - \theta)$ to decrease markedly so that it would take a very large ratio of k_1/k_2 to make the term k$_2\theta$ negligible at high coverage. Thus, the corrosion rates of many inhibited systems at high coverage do no suggest simply the high degree of adsorption but rather a new expression, i.e., simply $k_2\theta$. In such cases, the term $k_1 (1 - \theta)$ will be negligible and the corrosion mechanism probably involves direct reaction of the species 'metal atom-adsorbed inhibitor molecules'. It is thus probable that the activation energy in $k_2 = \lambda e^{-\Delta E_2/RT}$ will be quite different from that in the uninhibited rate constant
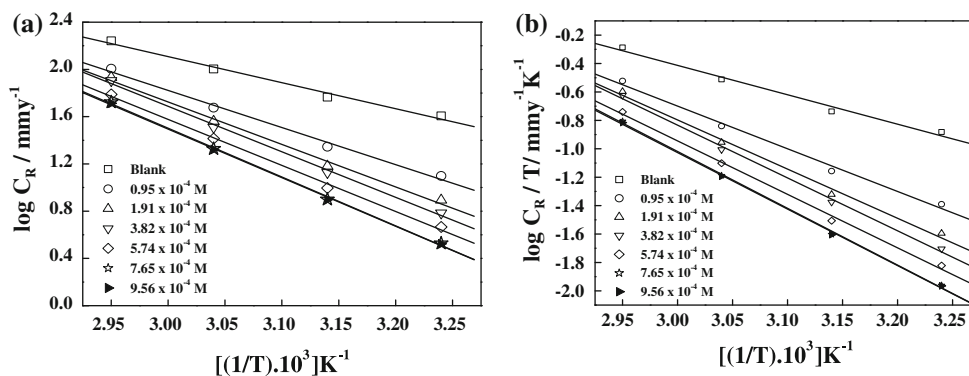

Fig. 3 **a** Adsorption isotherm plot for log (C_R) versus $1/T$; **b** Adsorption isotherm plot for log (C_R/T) versus $1/T$

Table 3 Corrosion rate constant, k_1 and k_2, values obtained as a function of the covered metal surface

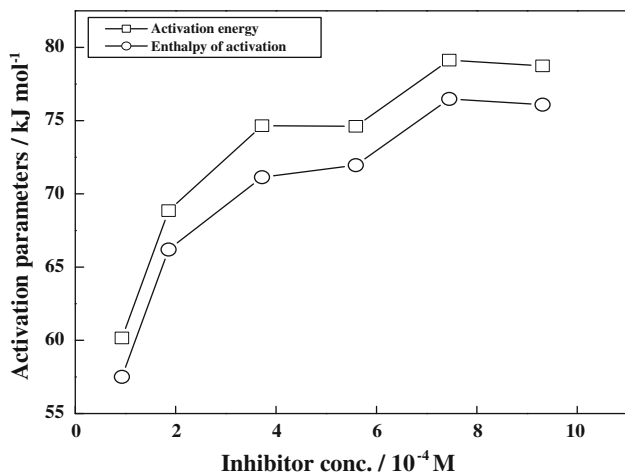| Temperature (K)	k_1	k_2	R^2
308	40.22	0.076	0.999
318	58.23	0.003	1.000
328	100.89	0.013	1.000
338	174.58	0.001	1.000

Fig. 4 Variation of activation parameters with different concentrations of ceftobiprole

k_1. Thus it is possible that the activation energy of inhibited reaction at high coverage can be either larger or smaller than that of the uninhibited reaction. The trend of activation energies in the present work may be followed in this way.

The relationship between log (C_R/T) and $1/T$ was shown in Fig. 3b. Straight lines are obtained with a slope $(-\Delta H^*/2.303R)$ and an intercept of $[\log(R/Nh)+ (\Delta S^*/2.303R)]$, from which the value of ΔH^* and ΔS^* were calculated and presented in Table 2.

The relationship between activation energy and enthalpy of activation against the concentration of ceftobiprole is shown in Fig. 4. From the data obtained in Table 2, it is clear that E_a, ΔH^* vary in the same manner. In the presented study, activation parameters increase first with increasing concentration and at higher concentration are almost constant. In this case, there was no dramatic change in the value of λ, and therefore the decrease in corrosion rate is mainly controlled by activation parameters.

On comparing the values of entropy of activation (ΔS^*) listed in Table 2, it is clear that entropy of activation increased in presence of ceftobiprole compared to free acid solution. Such variation is associated with the phenomenon of ordering and disordering of inhibitor molecules on the mild steel surface. The increase of entropy of activation in the presence of ceftobiprole indicated that increase in

disorderness takes place on going from reactant to activated complex.

3.2 Thermodynamic parameters and adsorption isotherm

The adsorption on the corroding surfaces never reaches the real equilibrium and tends to reach an adsorption steady state. When corrosion rate is sufficiently decreased in the presence of inhibitor, the adsorption steady state has a tendency to attain quasi-equilibrium state. Now, it is reasonable to consider quasi-equilibrium adsorption in thermodynamic way using the appropriate adsorption isotherm. The degree of surface coverage (θ) for inhibitor was obtained from average weight loss data. Different adsorption isotherms were tested in order to find the best suitable adsorption isotherm for adsorption of ceftobiprole on the surface of mild steel from 1 M HCl solution. Langmuir adsorption isotherm (Eq. 5) was found best fit (Fig. 5). The deviation of the slopes from unity can be attributed to the molecular interaction among the adsorbed inhibitor species, a factor which was not taken into consideration during the derivation of the Langmuir equation.

Though the linearity of Langmuir plot may be interpreted to suggest that the experimental data for ceftobiprole obey the Langmuir adsorption isotherm, the considerable deviation of the slope from unity showed that the isotherm can not be strictly applied.

With regard to the Langmuir adsorption isotherm the surface coverage (θ) of the inhibitor on the mild steel surface is related to the concentration (C_{inh}) of the inhibitor in the bulk of the solution according to the following equation:
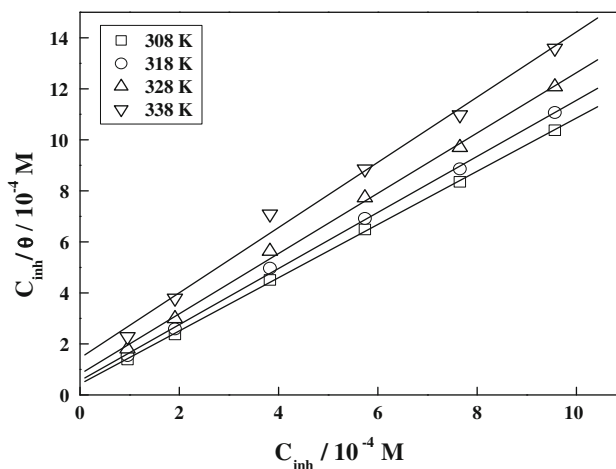

Fig. 5 Langmuir adsorption isotherms for the adsorption of ceftobiprole at different conc. in 1 M HCl on the surface of mild steel

$$\theta = \frac{K_{ads}C_{inh}}{1 + K_{ads}C_{inh}} \tag{5}$$

where, K_{ads} is the equilibrium constant for the adsorption/desorption process. This equation can be rearranged to

$$\frac{C_{inh}}{\theta} = \frac{1}{K_{ads}} + C_{inh} \tag{6}$$

It is known fact that K_{ads} represents the strength between adsorbate and adsorbent. Large values of K_{ads} imply more efficient adsorption and hence better inhibition efficiency [36].

From the intercepts of the straight lines on the C_{inh}/θ-axis (Fig. 5a), K_{ads} can be calculated which is related to free energy of adsorption, ΔG_{ads}^o, as given by Eq. 7.

$$\Delta G_{ads}^o = -RT \ln(55.5 K_{ads}) \tag{7}$$

The negative values of ΔG_{ads}^o ensure the spontaneity of the adsorption process and stability of the adsorbed layer on the mild steel surface [37, 38]. It is usually accepted that the value of ΔG_{ads}^o around -20 kJ mol^{-1} or lower indicate the electrostatic interaction between charged metal surface and charged organic molecules in the bulk of the solution while those around -40 kJ mol^{-1} or higher involve charge sharing or charge transfer between the metal surface and organic molecules [39].

Assuming thermodynamic model, corrosion inhibition of mild steel in the presence of ceftobiprole can be better explained, therefore, heat of adsorption and entropy of adsorption were calculated.

According to Van't Hoff equation [40]:

$$\ln K_{ads} = (-\Delta H_{ads}^o / RT) + \text{constant} \tag{8}$$

To calculate adsorption heat, $\ln K_{ads}$ was plotted against $1/T$, as shown in Fig. 6a. The straight lines were obtained with slope equal to $(-\Delta H_{ads}^o/R)$ and intercept equal to $(\Delta S_{ads}^o/R + \ln 1/55.5)$. The calculated values of heat of adsorption and entropy of adsorption are listed in Table 4. Under the experimental conditions, the adsorption heat could be approximately regarded as the standard adsorption heat (ΔH_{ads}^o).

The thermodynamic parameters ΔH_{ads}^o and ΔS_{ads}^o can also be calculated from the following equation:

$$\Delta G_{ads}^o = \Delta H_{ads}^o - T\Delta S_{ads}^o \tag{9}$$

A plot of ΔG_{ads}^o vs. T gives straight lines (Fig. 6b) with the slope equal to $-\Delta S_{ads}^o$, and the value of ΔH_{ads}^o can be calculated from intercept. Values of ΔH_{ads}^o and ΔS_{ads}^o obtained by both methods follow the same trend.

The sign of enthalpy of adsorption is negative in the presence of ceftobiprole. The values of entropy of
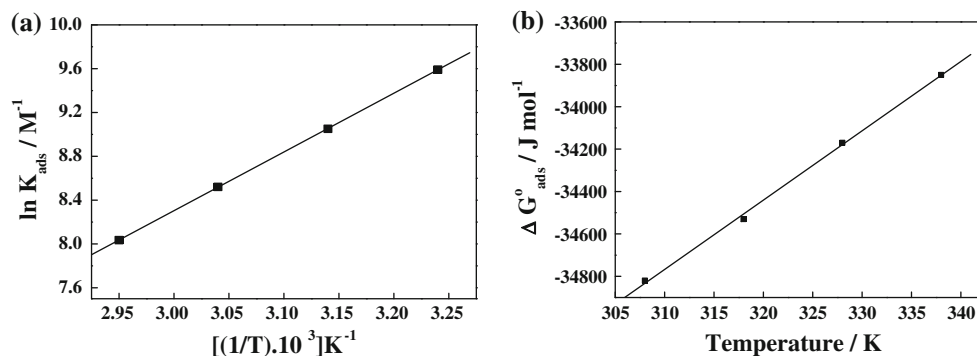

Fig. 6 Adsorption isotherm plot for a $\ln K_{ads}$ vs. $1/T$ and b ΔG_{ads}^o vs. T for adsorption of ceftobiprole on mild steel in 1 M HCl

Table 4 Thermodynamic parameters for the adsorption of ceftobiprole in 1 M HCl on the mild steel at different temperatures

Acid solution	Name of inhibitor	Conc. of inhibitor (M × 10^{-4})	Temperature (K)	K_{ads} (10^4 M^{-1})	$-\Delta G_{ads}^o$ (kJ mol^{-1})	$-\Delta H_{ads}^o$ (kJ mol^{-1})[a]	$-\Delta S_{ads}^o$ (J mol^{-1} K^{-1})[a]	$-\Delta H_{ads}^o$ (kJ mol^{-1})[b]	$-\Delta S_{ads}^o$ (J mol^{-1} K^{-1})[b]
1 M HCl	Ceftobiprole	7.45	308	1.46	34.82	44.53	31.22	44.90	32.7
			318	0.85	34.53	–	–	–	–
			328	0.50	34.17	–	–	–	–
			338	0.31	33.85	–	–	–	–

[a] Calculated from Eq. 8

[b] Calculated from Eq. 9

adsorption are also negative. In fact, it is well known fact that adsorption is an exothermic phenomenon accompanied by a decrease in entropy [41]. Inspection of Table 4 revealed that decrease in enthalpy and entropy are the driving force for the adsorption of ceftobiprole on the mild steel surface.

3.3 Electrochemical impedance spectroscopy

Electrochemical impedance measurements were carried over the frequency range from 100 kHz to 0.01 Hz at open circuit potential. EIS behaviour of ceftobiprole at different concentration is shown in Fig. 7a–c.

Inhibition efficiency can be calculated from Nyquist plot as follows:

$$\mu_{R_{ct}\%} = \frac{R_{ct}^{i} - R_{ct}^{0}}{R_{ct}^{i}} \times 100 \tag{10}$$

where, R_{ct}^{i} and R_{ct}^{0} are the charge transfer resistance of mild steel with and without inhibitor molecules, respectively. Inhibition efficiencies and other calculated impedance parameters presented Table 5.

The impedance response of mild steel in acid solution was significantly changed after the addition of ceftobiprole,

and the impedance of the inhibited system increased with inhibitor concentration. Furthermore, at 7.45×10^{-4} M concentration of ceftobiprole gives rise to much larger semicircle diameter than other two lower concentrations of ceftobiprole (Fig. 7a). In the presence of ceftobiprole, in the completely studied concentration interval, the electrochemical impedance spectra in complex plane presentation (Nyquist diagram) are characterized by one depressed semicircle, with a high frequency capacitive loop and low frequency inductive loop. Deviation from perfect circular shape, often known as frequency dispersion, was attributed to surface roughness and inhomogeneities of the solid surface [42, 43]. The high frequency capacitive loop may be due to a charge transfer process. The low frequency inductive loop can be attributed to bulk relaxation process of the adsorbed compound [44].

Figure 8 showed the electrical equivalent circuit employed to analyse the impedance spectra. Excellent fit with this model was obtained for all experimental data. As an example, the Nyquist and Bode plots for ceftobiprole at 7.45×10^{-4} M in 1 M HCl are presented in Fig. 9a and b, respectively. The measured and simulated data fitted very well. It is observed that the fitted data follow almost the same pattern as the original results
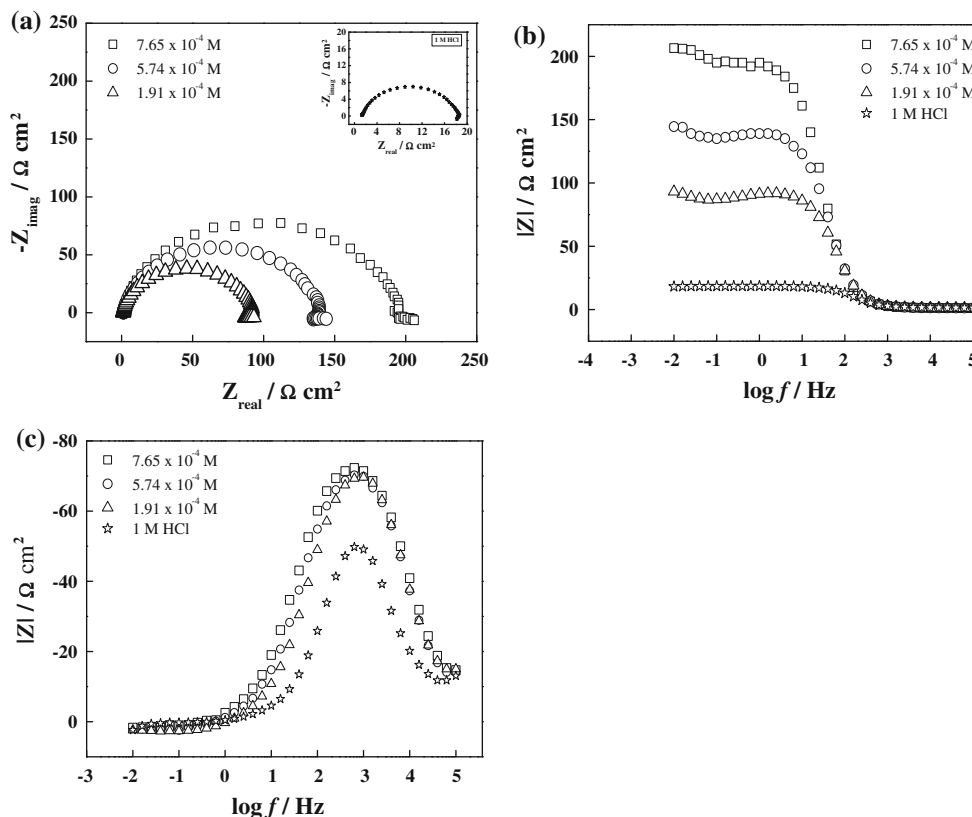

Fig. 7 Typical **a** Nyquist, **b** Bode-magnitude and **c** impedance-phase plots obtained for the mild steel in 1 M HCl in the absence and presence of different concentrations of ceftobiprole

Table 5 Impedance parameters and inhibition efficiency values for mild steel after 30 min immersion period in 1 M HCl in absence and presence of different concentrations of ceftobiprole

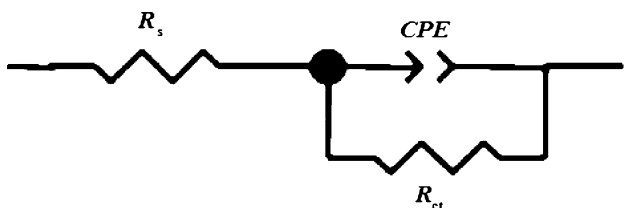| Acid solution	Conc. of inhibitor (M × 10^{-4})	R_s (Ω cm^2)	R_{ct} (Ω cm^2)	Y_0 (μF cm^{-2})	n	C_{dl} (μF cm^{-2})	$\mu_{R_{ct}}$%
1 M HCl	–	1.32	17.24	162.00	0.845	55.09	–
	1.86	1.03	89.21	51.16	0.884	25.22	80.67
	5.59	1.20	137.10	46.28	0.889	24.60	87.42
	7.45	1.08	196.30	40.19	0.899	23.32	91.21

Fig. 8 Electrochemical equivalent circuit used to fit the impedance spectra
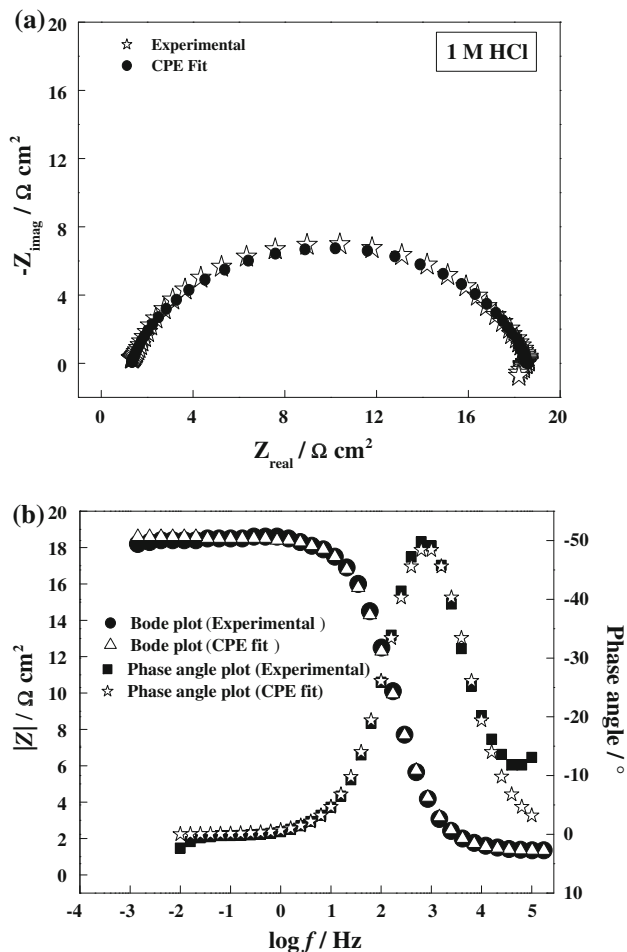

Fig. 9 a Nyquist plot of iron corrosion in 1 M HCl solution and **b** Bode-phase plots of iron corrosion in 1 M HCl solution

along the whole diagrams. The high frequency part of the impedance and phase angle describes the behaviour of an inhomogeneous surface layer, while the low frequency contribution shows the kinetic response for the charge transfer reaction [45].

Phase angle at high frequencies provides a general idea of anticorrosion performance. The more negative the phase angle the more capacitive the electrochemical behaviour [46]. Depression of phase angle at relaxation frequency occurs with decreasing ceftobiprole concentration which indicated the decrease of capacitive response with the decrease of inhibitor concentration (Fig. 7c). Such a phenomenon could be attributed to higher corrosion activity at low concentrations of inhibitors.

To get more accurate fit of these experimental data, constant phase element has used instead of capacitive element. The CPE impedance is given by [47]:

$$Z_{CPE} = Y_0^{-1} (i\omega)^{-n} \tag{11}$$

where, Y_0 is the CPE constant, ω is the angular frequency (in rad s^{-1}), $i^2 = -1$ is the imaginary number and n is a CPE exponent which can be used as a gauge of the heterogeneity or roughness of the surface [48]. Depending on the value of n, CPE can represent resistance ($n = 0$, $Y_0 = R$), capacitance ($n = 1$, $Y_0 = C$), inductance ($n = -1$, $Y_0 = L$) or Warburg impedance ($n = 0.5$, $Y_0 = W$).

The electrochemical parameters, including R_s, R_{ct}, Y_0 and n, obtained from fitting the recorded EIS data using the equivalent circuit of Fig. 8, were listed in Table 5. C_{dl} values derived from CPE parameters according to Eq. 12 were also listed in Table 3.

$$C_{dl} = (Y_0 \cdot R_{ct}^{1-n})^{1/n} \tag{12}$$

Inspection of the results in Table 5 indicated that the R_{ct} value increased with the concentration of ceftobiprole. The increase in R_{ct} value is attributed to the formation of protective film on the metal/solution interface. Indeed, the increase of the values of n when compared with 1 M HCl and with ceftobiprole concentration can be explained by some decrease of the surface heterogeneity, due to the adsorption of the inhibitor on the most active adsorption sites [49]. Moreover, the values of double-layer capacitance, C_{dl}, decreased with increasing ceftobiprole concentration. The thickness of the protective layer (d) is related to C_{dl} according to the following equation [50]:

$$C_{dl} = \frac{\varepsilon \, \varepsilon_0}{d} \tag{13}$$

where, ε is the dielectric constant of the protective layer and ε_0 is the permittivity of free space.

It is obvious from the results that the ceftobiprole inhibited the corrosion of mild steel in 1 M HCl solution at all concentrations used in this study and the $\mu_{R_{ct}}\%$ was seen to increase continuously with increasing additive concentration at 303 K (Table 5). The inhibition efficiencies, calculated from ac impedance results, show the same trend as those obtained from weight loss measurements.

3.4 Linear polarization resistance

Polarization resistance values were determined from the slope of the potential-current lines,

$$R_{\mathrm{p}} = A \frac{dE}{di} \tag{14}$$

where, A is the surface area of the electrode, dE is change in potential and di is change in current. The R_{p} values were used to calculate the inhibition efficiencies, ($\mu_{R_{\mathrm{p}}}\%$) using the relationship:

$$\mu_{R_{\mathrm{p}}}\% = \frac{R_{\mathrm{p}}^{\mathrm{i}} - R_{\mathrm{p}}^{0}}{R_{\mathrm{p}}^{\mathrm{i}}} \times 100 \tag{15}$$

where, $R_{\mathrm{p}}^{\mathrm{i}}$, and R_{p}^{0} are the polarization resistances in the presence and absence of inhibitor, respectively. The inhibition efficiencies and polarization resistance parameters presented Table 6.

3.5 Tafel polarization

The values of corrosion potential (E_{corr}), corrosion current density (i_{corr}), anodic and cathodic Tafel slopes (β_{a} and β_{c}) can be evaluated from anodic and cathodic regions of Tafel plots. The linear Tafel segments of anodic and cathodic curves were extrapolated to corrosion potential to obtain corrosion current densities (i_{corr}).

The inhibition efficiency was evaluated from the measured i_{corr} values using the relationship:

$$\mu_{\mathrm{p}}\% = \frac{i_{\mathrm{corr}}^{\mathrm{o}} - i_{\mathrm{corr}}'}{i_{\mathrm{corr}}^{\mathrm{o}}} \times 100 \tag{16}$$
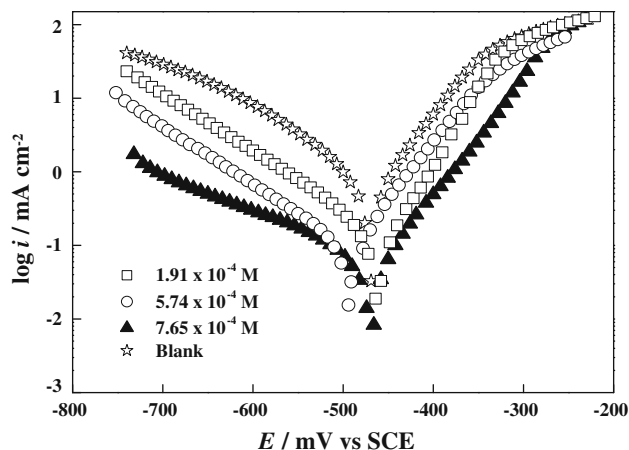

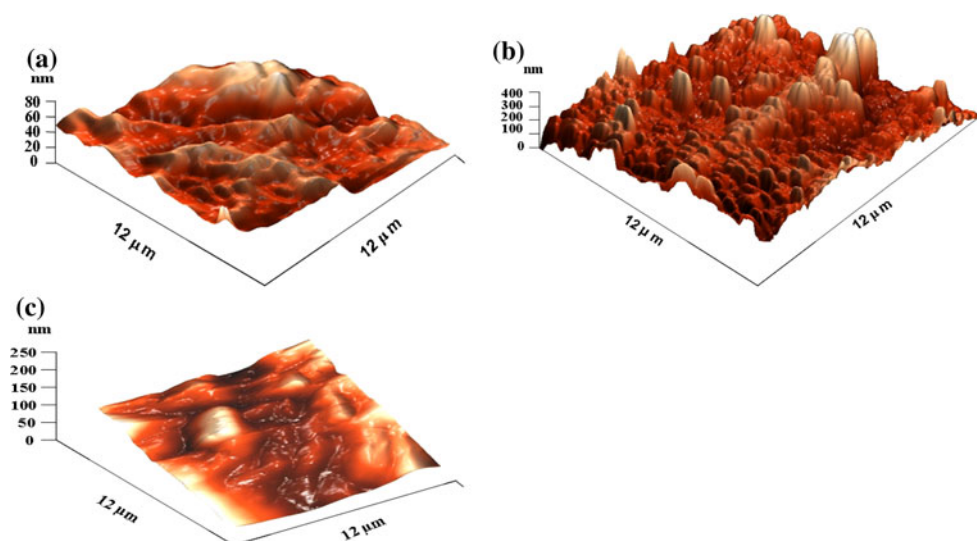**Fig. 10** Tafel Polarization behaviour of mild steel in 1 M HCl with different concentration range of ceftobiprole

where, $i_{\mathrm{corr}}^{\mathrm{o}}$ and $i_{\mathrm{corr}}^{\mathrm{i}}$ are values of corrosion current density in absence and in presence of inhibitor, respectively.

Figure 10 represented the potentiodynamic polarization curves of mild steel in 1 M HCl in the absence and presence of various concentrations of the ceftobiprole. It can be seen from the Fig. 10 that, in the presence of inhibitor, the curves are shifted to lower current regions, showing the inhibition tendency of the ceftobiprole. There was no definite trend is observed in the E_{corr} values in the presence of ceftobiprole. In the present study, shift in E_{corr} values is in the range of 20–25 mV suggested that they all are acted as mixed type of inhibitor [51, 52]. The values of various electrochemical parameters derived by Tafel polarization of all the inhibitors are given in Table 6. Investigation of Table 6 revealed that the values of β_{a} change slightly in the presence of ceftobiprole where as more pronounced change occurs in the values of β_{c}, indicating that both anodic and cathodic reactions are effected but the effect on the cathodic reactions is more prominent. Thus, ceftobiprole acted as mixed type, but predominantly cathodic inhibitor [53]. Increase in inhibition efficiencies with increasing concentration of ceftobiprole reveals that inhibition action is due to adsorption on steel surface and the adsorption is known to depend on the chemical structure of the inhibitors.

Table 6 Potentiodynamic polarization parameters for mild steel without and with different concentrations of ceftobiprole in 1 M HCl

Acid solution	Conc. of inhibitor (M × 10^{-4})	Linear polarization		Tafel Polarization				
		R_{p} (Ω cm^2)	$\mu_{R_{\mathrm{p}}}\%$	E_{corr} (mV vs. SCE)	i_{corr} (μA cm^{-2})	β_{a} (mV/dec)	β_{c} (mV/dec)	$\mu_{\mathrm{P}}\%$
1 M HCl	0	18.69	–	−469	730	73	127	–
	1.86	94.5	80.21	−462	149	74	116	79.5
	5.59	137.8	86.42	−489	129	70	171	82.3
	7.45	210.6	91.12	−469	69	80	185	90.5

The inhibition efficiencies of investigated compound obtained by weight loss, polarization resistance and Tafel polarization methods are in good agreement.

3.6 Surface characterization: AFM study

To establish whether inhibition is due to the formation of a film on the metal surface via adsorption, atomic force micrographs were taken. The three-dimensional AFM images are shown in Fig. 11a–c. As can be seen from Fig. 11a–c, there was much less damage on the surface of mild steel with ceftobiprole. The average roughness of polished mild steel (Fig. 11a) and mild steel in 1.0 M HCl without inhibitor (Fig. 11b) was calculated to be 66 and 395 nm, respectively. The mild steel surface in the free acid solution is getting
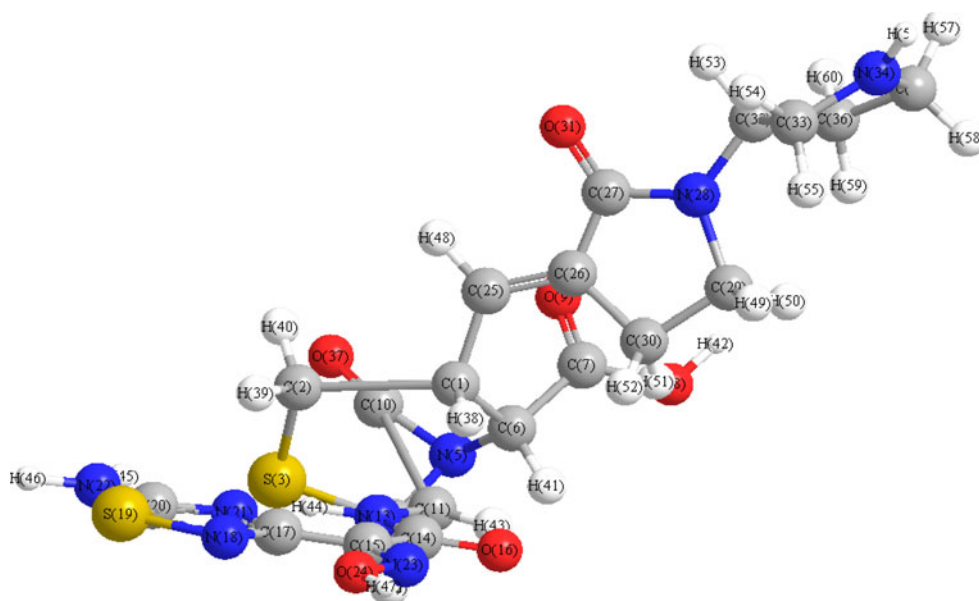
cracked due to the acid attack on the surface (Fig. 11b). However, in presence of 7.45 × 10^{-4} ppm concentration of ceftobiprole, the average roughness was reduced to 185 nm in the presence of ceftobiprole (Fig. 11c).

4 Mechanism of inhibition

From the results obtained from different electrochemical and weight loss measurements, it was concluded that ceftobiprole inhibited the corrosion of mid steel in 1 M HCl by adsorption at mild steel/solution interface.

It is general assumption that the adsorption of organic inhibitors at the metal surface interface is the first step in the mechanism of the inhibitor action. Organic molecules may adsorbed on the metal surface in four types namely,

Fig. 12 Three-dimensional representation of ceftobiprole molecule

(i) Electrostatic interaction between the charged molecules and the charged metal,
(ii) Interaction of unshared electron pairs in the molecule with the metal,
(iii) Interaction of π-electrons with the metal and
(iv) a combination of types (i–iii) [54, 55].

The inhibition of active dissolution of the metal is due to the adsorption of the inhibitor molecules on the metal surface forming a protective film. The inhibitor molecules can be adsorbed on to the metal surface through electron transfer from the adsorbed species to the vacant electron orbital of low energy in the metal to form a co-ordinate type link.

The inhibition efficiency depends on many factors [56, 57] including the number of adsorption centres, mode of interactions with metal surface, molecular size and structure.

It is well known that iron has co-ordination affinity towards nitrogen, sulphur and oxygen bearing ligands [58, 59]. Hence, adsorption on iron can be attributed to co-ordination through iminic group, hetero atom (N and S) and π-electrons of aromatic ring.

In acidic solution, carbonyl group (O_{16}), secondary amine group (N_{13}), free amino group (N_{22}), iminic nitrogen (N_{23}) as well as nitrogen atoms in thiadiazole ring are protonated easily because all of them are planar and having high electron density (Fig. 12). Physical adsorption may take place due to electrostatic interaction between protonated molecule and $(FeCl^-)_{ads}$ species. Interaction between mild steel surface and unshared electron pairs of N-atoms and unprotonated S-atom occurs due to co-ordinate covalent bond formation. Another striking feature for high inhibition performance of ceftobiprole is the presence of S-atom. The presence of S-atom in the inhibitor structures makes the formation of $d\pi$–$d\pi$ bond resulting from overlap of 3d-electrons from iron atom to the 3d vacant orbital of S-atom possible, which enhances the adsorption of the compounds on the metal surface. Chemical adsorption of ceftobiprole is also possible due to interaction of π-electrons with metal surface following deprotonisation step of the physically adsorbed protonated molecules.

The results obtained from weight loss, EIS, linear polarization and Tafel polarization are in a good agreement.

5 Conclusions

The corrosion behaviour of mild steel was investigated in 1 M HCl with and without addition of various concentrations of ceftobiprole using weight loss, EIS, linear polarization and potentiodynamic polarization. The main conclusions are:

1. The adsorption of ceftobiprole obeyed Langmuir adsorption isotherm.
2. Ceftobiprole acted as mixed type inhibitor.
3. Decrease in enthalpy and entropy are the driving force for the adsorption of ceftobiprole on the mild steel surface.
4. The inhibition efficiency of ceftobiprole decreased with temperature, which leads to an increase in activation energy of corrosion process.
5. The increase in CPE exponent (n) with increasing concentration of ceftobiprole indicated that the surface roughness of mild steel decreased with increasing inhibitor concentration.

References

1. Badr GE (2009) Corros Sci 51:2529
2. Ren Y, Luo Y, Zhang K, Zhu G, Tan X (2008) Corros Sci 50:3147
3. Jacob KS, Parameswaran G (2009) Corros Sci. doi:10.1016/j.corsci.2009.09.007
4. Abd El-Maksoud SA, Fouda AS (2005) Mater Chem Phys 93:84
5. Ju H, Kai ZP, Li Y (2008) Corros Sci 50:865
6. Mu G, Li X (2005) J Colloid Interface Sci 289:184
7. Oguzie EE, Li Y, Wang FH (2007) J Colloid Interface Sci 310:90
8. Lece HD, Emregul KC, Atakol O (2008) Corros Sci 50:1460
9. Morad MS, Kamal El-Dean AM (2006) Corros Sci 48:3398
10. Aljourani J, Raeissi K, Golozar MA (2009) Corros Sci 51:1836
11. Lebrini M, Traisnel M, Lagrenee M, Mernari B, Bentiss F (2008) Corros Sci 50:473
12. Wanees SAE, Abd El Aal EE (2009) Corros Sci. doi:10.1016/j.corsci.2009.09.022
13. Damaskin BB, Frumkin AN (1971) In: Hush NS (ed) Adsorption of molecules on electrodes. Wiley-Interscience, London, p 1
14. Singh AK, Quraishi MA (2009) Corros Sci 51:2752
15. Christov M, Popova A (2004) Corros Sci 46:1613
16. Fouda AS, Mostarfa HA, El-Taib F, Elewady GY (2005) Corros Sci 47:1988
17. Prabhu RA, Shanbhag AV, Venkatesha TV (2007) J Appl Electrochem 37:491
18. Li X, Deng S, Fu H, Li T (2009) Electrochim Acta 54:4089
19. Moretti G, Guidi F, Grion G (2004) Corros Sci 46:387
20. Ferreira ES, Giacomelli C, Giacomelli FC, Spinelli A (2004) Mater Chem Physd 83:129
21. Morad MS (2008) Corros Sci 50:436
22. Singh AK, Quraishi MA (2009) Corros Sci 52:152
23. Shukla SK, Singh AK, Ahamad I, Quraishi MA (2009) Mater Lett 63:819
24. El-Naggar MM (2007) Corros Sci 49:2226
25. Abdallah M (2004) Corros Sci 46:1981
26. Obot IB, Obi-Egbedi NO, Umoren SA (2009) Corros Sci 51:1868
27. Mathur PB, Vasudevan T (1982) Corrosion 38:171
28. Quraishi MA, Ansari FA (2003) J Appl Electrochem 33:233
29. Quraishi MA, Ahamad I, Singh AK, Shukla SK, Lal B, Singh V (2008) Mater Chem Phys 112:1035
30. Shukla SK, Quraishi MA (2009) Corros Sci 51:1007
31. Li XH, Deng SD, Fu H, Mu GN (2008) Corros Sci 50:2635

32. Soltani N, Behpour M, Naiemi H (2009) Corros Sci. doi:
    10.1016/j.corsci.2009.11.045
33. Szauer T, Brand A (1981) Electrochim Acta 26:1219
34. Riggs OL Jr, Hurd RM (1967) Corrosion 23:252
35. O'M Bockris J, Drazic D (1962) Electrochim Acta 7:293
36. Singh AK, Quraishi MA (2010) J Appl Electrochem 40:1293
37. Keles H, Keles M, Dehri I, Serindag O (2008) Colloids Surf A
    320:138
38. Fouda AS, Heakal FE, Radwan MS (2009) J Appl Electrochem
    39:391
39. Moretti G, Quartarone G, Tassan A, Zingales A (1996) Electro-
    chim Acta 41:1971
40. Tang L, Mu G, Liu G (2003) Corros Sci 45:2252
41. Li X, Deng S, Fu H, Mu G (2009) Corros Sci 51:620
42. Tao Z, Zhang S, Li W, Hou B (2009) Corros Sci. doi:
    10.1016/j.corsci.2009.06.042
43. Lenderink JW, Linden M, Wit JH (1993) Electrochim Acta
    39:1989
44. Aoki IV, Guedes IG, Maranho SL (2002) J Appl Electrochem
    32:915
45. Khaled KF (2003) Electrochim Acta 48:2493
46. Mahadavian M, Attar MM (2006) Corros Sci 48:4152
47. Qu Q, Jiang S, Bai W, Li L (2007) Electrochim Acta 52:6811
48. Alvarez-Bustamante R, Negrón-Silva G, Abreu-Quijano M,
    Herrera-Hernández H, Romero-Romo M, Cuán A, Palomar-
    Pardave M (2009) Electrochim Acta 54:5393
49. Lebrini M, Lagrenee M, Vezin H, Traisnel M, Bentiss F (2007)
    Corros Sci 49:2254
50. Hassan HH (2006) Electrochim Acta 51:5966
51. Riggs OL Jr (1973) Corrosion inhibitors, 2nd edn. C.C. Nathan,
    Houston, TX
52. Singh AK, Quraishi MA (2009) Corros Sci. doi:10.1016/j.
    corsci.2009.12.011
53. Khaled KF, Hackerman N (2003) Electrochim Acta 48:2715
54. Schweinsberg DP, George GA, Nanayakkara AK, Steiner DA
    (1988) Corros Sci 28:33
55. Shorky H, Yuasa M, Sekine I, Issa RM, El-Baradie HY, Gomma
    GK (1998) Corros Sci 40:2173
56. Noor EA (2005) Corros Sci 47:33
57. Bentiss F, Jama C, Mernari B, El Attari H, El Kadi L, Lebrini M,
    Traisnel M, Lagrenee M (2009) Corros Sci 51:1628
58. Ali SA, Al-Muallem HA, Rahman SU, Saeed MT (2008) Corros
    Sci 50:3070
59. Lowmunkhong P, Ungthararak D, Sutthivaiyakit P (2009) Corros
    Sci. doi:10.1016/j.corsci.2009.08.039